Electron Demagnetization in a Magnetically Expanding Plasma

Justin M. Little
Space Propulsion and Advanced Concepts Engineering (SPACE) Laboratory, University of Washington, Seattle, Washington 98015, USA

Edgar Y. Choueiri
Electric Propulsion and Plasma Dynamics Laboratory (EPPDyL), Princeton University, Princeton, New Jersey 08544, USA

(Received 25 April 2019; revised manuscript received 13 August 2019; published 2 October 2019)

Electron demagnetization in a magnetically expanding plasma, a fundamental process for plasma flow and detachment in magnetic nozzles, is experimentally investigated using a rf plasma source and magnetic nozzle (MN). Measurements of the plasma potential spatial profile reveal an ion-confining potential surface, indicative of the edge of a magnetized plasma, that extends along the outermost magnetic flux surface. The downstream extent of the potential surface scales inversely with a characteristic electron Larmor radius, which agrees with an existing theory [E. Ahedo and M. Merino, Phys. Plasmas **19**, 083501 (2012)] for electron demagnetization via finite electron Larmor radius (FELR) effects. These results represent the first experimental evidence of FELR demagnetization, and provide an empirical metric for the significance of FELR effects based on the degree of separation between electron and magnetic flux surfaces. With this metric, a critical magnetic field strength is found that ensures electrons remain magnetized through the MN turning point, thus avoiding the rapid plume divergence associated with premature demagnetization.

DOI: 10.1103/PhysRevLett.123.145001

Plasma flow along an expanding magnetic field, in addition to being a naturally occurring phenomenon in the solar wind [1] and astrophysical jets [2], also plays a significant role in plasma processing [3] and propulsion technologies [4–6]. The nature by which the plasma flow decouples (i.e., detaches) from the magnetic field is fundamentally important as it marks the transition between magnetized and unmagnetized flow regimes, thus impacting a variety of critical physics such as mass and energy transport [7], instability growth [8], and wave propagation [9]. Detachment is especially important for space electric propulsion concepts that utilize magnetic nozzles (MNs) [10] because plasma propellant returning along the magnetic field degrades performance and represents a hazard to sensitive spacecraft components.

Theories for MN plasma detachment have been proposed based on a variety of physical processes, including collisions [11,12], instabilities [13,14], finite Larmor radius effects [15,16], and magnetic field perturbations [17,18]. Experiments have shown that the ion streamlines and plasma density profile diverge less than the downstream magnetic field [13,19–21], in agreement with theoretical models [22]. Despite its importance, experimental investigation into electron demagnetization in the downstream region is notably absent from the literature. In this Letter, we experimentally examine electron dynamics in a MN using measurements of the plasma potential profile, and use the resulting insight to answer the question: what is the cause and consequence of electron demagnetization in a magnetically expanding plasma?

Experiments were performed using an 18.5 cm long, 7.5 cm diameter rf plasma source (PS) mounted inside a 7.6 m long, 2.4 m diameter dielectric vacuum chamber (Fig. 1). The MN consisted of two electromagnetic coils ($r_c = 7.51$ cm) positioned near the exit of the PS. The field strength at the center of the MN, B_0, was controlled with the coil current, I_B, such that $B_0[\mathrm{G}] \approx 21 I_B[\mathrm{A}]$. Data were obtained at a fixed rf frequency, delivered power, argon

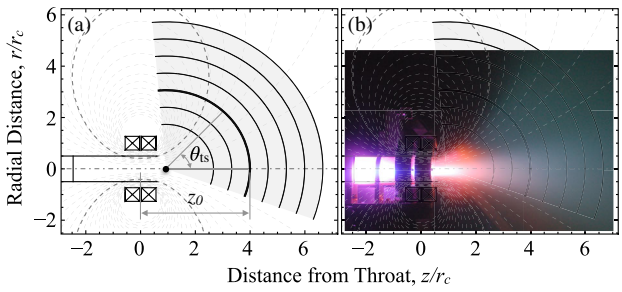

FIG. 1. (a) Schematic of the plasma source, electromagnets, magnetic field lines (dashed), intersecting magnetic field line (dashed bold), probe range (shaded), and measurement arcs (solid arcs). (b) Photograph of the operating plasma source ($P = 500$ W, $\dot{m} = 2$ mg/s) and magnetic nozzle ($I_B = 20$ A).

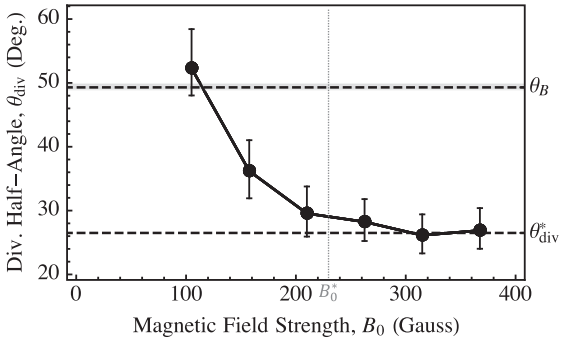

FIG. 2. Plume divergence decreases with increasing magnetic field strength. θ_B represents the divergence half-angle calculated assuming the ion streamtubes and magnetic field lines diverge at the same rate. θ^*_{div} represents the prediction from a two-fluid plasma model [32]. B_0^* coincides with $r_d = r_{tp}$.

mass flow rate, and background pressure of 13.56 MHz, 500 W, 0.5 mg/s, and ~20 μTorr, respectively. Detailed characterizations of the plasma source and downstream plasma can be found in Refs. [23,24].

Three diagnostics were used for this study: a rf-compensated Langmuir probe (LP) [25], emissive probe (EP) [26], and Faraday probe (FP) [27]. The LP provided the plasma density, n, and electron temperature, T_e. The EP provided the plasma potential, V_p, using the floating point method [26] and correcting for double sheath effects [28]. Additional details regarding probe construction, operation, and data analysis may be found in Refs. [24,29]. The FP, used to measure ion current density, consisted of a 6.0 mm diameter flat electrode surrounded by a 2.5 mm wide guard ring, both biased to −27 V. A guard ring was used to ensure the formation of a flat sheath in front of the collection electrode, thus reducing measurement error [27].

A translation stage (TS) was used to take measurements along an arc centered on the thruster exit. The TS was physically limited to $\theta_{ts} \in [-20, 95]$ degrees. Throughout this Letter, we will reference the downstream location of each sweep using the axial distance of the probe tip from the MN throat, z_0 [as shown in Fig. 1(b)]. Measurement sweeps were taken at seven equally spaced downstream locations within the range $z_0 \in [20, 50]$ cm.

From the FP measurement we calculate the ion streamtube locations [13] and plume divergence half-angle (θ_{div}) [30] as a function of B_0. Both the streamtubes [31] and divergence half-angle (Fig. 2) indicate that the ion beam divergence decreases as B_0 increases. For low B_0, the ion beam diverges more than the magnetic field ($\theta_{div} > \theta_B$). With increasing B_0 a transition occurs to $\theta_{div} < \theta_B$. Ultimately, θ_{div} asymptotes to a value that agrees with predictions from a two-fluid plasma model [32]. We note that θ_{div} is predicted to eventually increase with B_0 when the ion Larmor radius becomes much smaller than the plasma radius [16,33]; however, limitations to our magnet prevented us from accessing this regime.

Previous experiments have observed both inward [19,21] and outward [13] separation of the ion streamtubes with respect to MN field lines. Our measurements show that a transition from outward to inward separation exists as the MN field strength is increased. Theoretical models by Ahedo and Merino [16] predict that such a transition could result from finite electron Larmor radius (FELR) effects in the plume far field. Therefore, we seek to understand the electron response to changing magnetic field strength in our MN.

Plasma expansion along a diverging magnetic field for $T_e \gg T_i$ proceeds in the following manner [22]. Electrons created in the PS thermally expand along the magnetic field lines. To preserve quasineutrality a field-aligned potential gradient arises that draws ions from the PS and accelerates them in the downstream direction [34]. Electrons are confined to the magnetic flux tubes by virtue of their small Larmor radii. Through this confinement the electron pressure generates an azimuthal electron current that acts as the primary momentum transfer mechanism to the MN [35]. Ions are dominated primarily by electrostatic forces due to their large mass, and a potential gradient in the cross-field direction is produced pushing the ions outward to maintain quasineutrality near the edge of the plasma. Therefore, a cross-field potential gradient couples the electron and ion dynamics in a diverging magnetic field.

The field-aligned potential gradient in our experiment was presented along with ion velocity, electron density, and electron temperature measurements in Ref. [24], where we characterized electron cooling in a magnetically expanding plasma. We will now use the cross-field potential gradient to analyze the role of electron magnetization on MN plume divergence and plasma detachment. Figure 3(a) shows the plasma potential, V_p, measured from the EP as the probe is swept along a fixed-z_0 arc. Across most of the plume V_p

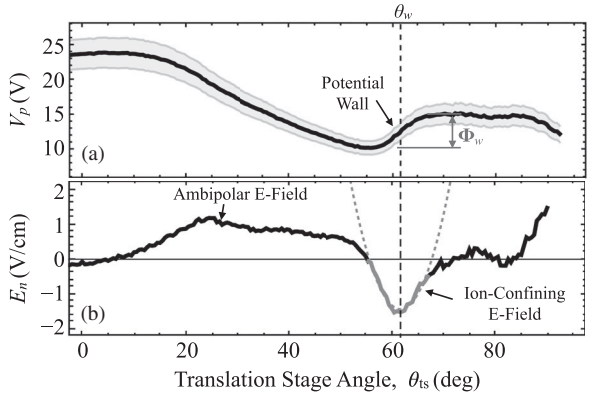

FIG. 3. (a) Plasma potential, V_p, measured along the $z_0 =$ 30 cm arc for $I_B = 15.0$ A. The shaded region indicates measurement uncertainty. (b) Electric field component along the probe arc, E_n. Highlighted data show the portion of the curve used to determine the potential wall location, θ_w.

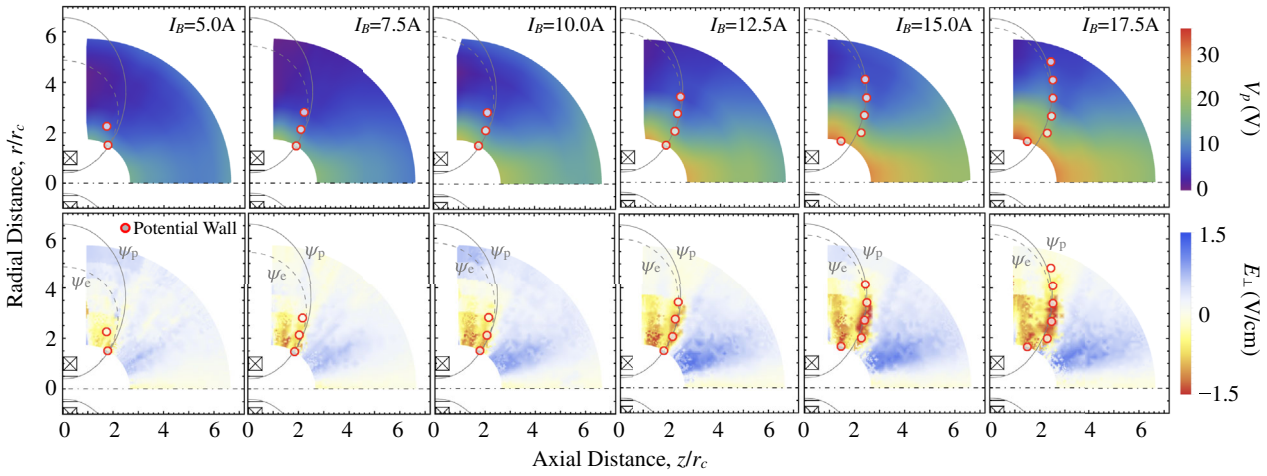

FIG. 4. Two-dimensional maps of the plasma potential (V_p) and perpendicular electric field ($E_\perp$) in the exhaust plume for increasing magnet currents, I_B. Also shown is the magnetic flux surface that intersects the plasma source wall, ψ_p, and outermost electron streamtube, ψ_e. The potential wall (red circles) is observed to closely follow ψ_p.

decreases with increasing θ_{ts}, which agrees with ambipolar plasma expansion theory [22]. A departure from this theory exists towards the plume boundary. Specifically, existing theoretical models predict V_p to monotonically decrease in the cross-field direction; however, our measurements show an increase in V_p near the plume edge. The "potential wall" formed in this region indicates a reversal in the direction of the electric field perpendicular to the magnetic field, thus generating an inward, confining force on the ions.

Maps of V_p and $E_\perp$ are presented in Fig. 4 for six different I_B. Here, $E_\perp = \vec{E} \cdot (\hat{e}_\theta \times \hat{e}_B)$ is the electric field component perpendicular to the magnetic field vector. Also shown is the magnetic flux surface that intersects the PS wall at the exit plane, labeled ψ_p, and the location of the potential wall along each probe arc, found by fitting a quadratic function to data in the ion-confining region [Fig. 3(b)]. These observations suggest that the potential wall in Fig. 3 is indicative of an ion-confining potential surface ($E_\perp < 0$) that forms along ψ_p and extends a distance that increases with I_B.

Similar potential surfaces have previously been reported in the literature [36,37]. Our measurements are the first to show the finite extent of the surface, including how this extent increases with magnetic field strength. Our findings are unique insofar as the potential surface along ψ_p *does not* coincide with a region of elevated plasma density [31]. This distinction can likely be attributed to differences in antenna geometry, background pressure, and wall proximity. Theoretical models predict inward electric fields can also manifest in expanding plasmas when $T_i \sim T_e$ [38]. Although T_i measurements were not taken in our experiment, comparable experiments find $T_i \sim 0.1$–0.5 eV [39,40]. This is further supported by our previous observation [24] that centerline measurements of T_e, V_p, and u_i in our experiment agree with expansion laws for $T_e \gg T_i$.

The potential surface we observe is consistent with charge separation at the plasma-vacuum (PV) interface [41,42]. The Larmor radius of the electrons and ions in the near-field expansion region satisfies $r_{L,e} \ll \ell_{\nabla B} < r_{L,i}$, where $\ell_{\nabla B} \equiv B/|\nabla B|$ is the magnetic field gradient scale length. In this regime, the magnetic field prevents electron cross-field motion whereas the ion motion is largely unaffected. As a result, ions with a significant cross-field velocity at the plasma edge can overshoot the PV interface, leading to a positive buildup of space charge and producing a region of $E_\perp < 0$. Therefore, existence of the ion-confining potential surface requires electrons to be magnetized near the edge of the plume, suggesting that its disappearance coincides with the point where electrons demagnetize. We now turn to an existing theoretical model to test this hypothesis and examine its scaling.

Ahedo and Merino use a two-fluid plasma model to show that FELR effects drive an outward separation of electron streamtubes relative to magnetic flux tubes in a magnetically expanding plasma [16]. We apply their analysis and examine the separation of the outermost electron streamtube, ψ_e. Conservation of angular momentum and isorotation along ψ_e can be expressed as $m_e r u_{\theta e} - e\psi = D(\psi_e)$ and $u_{\theta e}/r = w_{\theta e}(\psi_e)$, respectively. The combination of these conserved quantities yields the following transcendental equation for the location of ψ_e:

$$\psi(r_e, z_e) = \psi_p - \frac{m_e r_0 u_{\theta e,0}}{e}\left[\left(\frac{r_e}{r_0}\right)^2 - 1\right]. \quad (1)$$

Here, (r_e, z_e) represent the spatial coordinates of ψ_e, $u_{\theta e,0}$ is the electron azimuthal velocity at $(r_0, 0)$, and $\psi(r_0, 0) = \psi_p$. To calculate $u_{\theta e,0}$, we employ a subsequent analysis by Merino and Ahedo that incorporates an isotropic scaling law for T_e [38]. Electron momentum

conservation yields $u_{\theta e,0} = -r_0 H_e'(\psi_p)/e$, where $H_e(\psi) = \gamma_e k_b T_e/(\gamma_e - 1) - eV_p$. Because $dV_p/d\psi \approx 0$ at $z = 0$ in our experiment, we can calculate (r_e, z_e) using γ_e and measurements of $T_{e,t}(r) = T_e(r, 0)$. The electron polytropic index was found in a previous study [24] to be $\gamma_e = 1.15 \pm 0.03$. LP measurements determined that the shape of the T_e profile satisfies $\hat{T}_{e,t} = \exp[-\hat{r}^2/(2\hat{\sigma}_T^2)]$, where $\hat{T}_e \equiv T_{e,t}(r)/T_{e,0}$, $\hat{r} \equiv r/r_c$, and $\hat{\sigma}_T = 0.19 \pm 0.04$. Here, the uncertainties in γ_e and $\hat{\sigma}_T$ also account for their variation with I_B.

The location of ψ_e is shown in Fig. 4 along with the outermost magnetic flux tube, ψ_p, and potential wall locations. In agreement with Ahedo and Merino [16], we observe ψ_e to follow ψ_p in the near-field region, followed by an eventual outward separation of ψ_e with respect to ψ_p. We quantify the electron streamtube separation by introducing the parameter $\epsilon_\psi = (\psi - \psi_p)/\psi_p$, where ψ is evaluated along ψ_e. We assume for the moment that electron demagnetization occurs when the streamtube separation exceeds a critical value, ϵ_ψ^*. To understand the scaling of FELR demagnetization, we define a demagnetization radius, r_d, which describes the radius of the outermost electron streamtube at the point where $\epsilon_\psi = \epsilon_\psi^*$. From Eq. (1), it is straightforward to show that

$$\frac{r_d}{r_0} = \sqrt{1 + \frac{\epsilon_\psi^* r_0 \ell_{\nabla T}}{2\rho_{L,0}^2}\left(\frac{\gamma_e - 1}{\gamma_e}\right)}. \tag{2}$$

Here, $\ell_{\nabla T} = |d\hat{T}_{e,t}/dr|^{-1}_{r=r_p}$ and $\rho_{L,0} = \sqrt{m_e k_b T_{e,0}}/(eB_0)$ represent the electron temperature gradient length scale and characteristic Larmor radius, respectively. In the limit where $(r_d/r_0)^2 \gg 1$, Eq. (2) predicts that the demagnetization radius scales inversely with the characteristic electron Larmor radius.

Experimentally, we define r_d as the radius at which the ion confining potential wall disappears. We apply a linear regression to the Φ_w vs z_0 dataset and extrapolate the resulting line to $\Phi_w = 0$ [43]. The value of z_0 corresponding to $\Phi_w = 0$ is then used along with the arc geometry to calculate r_d. The measured values of r_d versus $\rho_{L,0}$ are shown in Fig. 5(a) along with the scaling law predicted from Eq. (2). The measured trend generally agrees with the predictions of FELR demagnetization theory to within the experimental uncertainty. Regression analysis yields $\epsilon_\psi^* \approx 0.04$, which provides a metric for how much streamtube separation can occur before electron FELR effects become significant. Disagreement between the theory and experiment is observed at high $\rho_{L,0}$, which can partly be explained by uncertainties in $\hat{\sigma}_T$ and γ_e [see the shaded region in Fig. 5(a)]. It is possible that reduced ionization in the PS at lower magnetic field strengths [23] produces effects not accounted for in the derivation of Eq. (2), such as ionization in the downstream region and collisional effects [44].

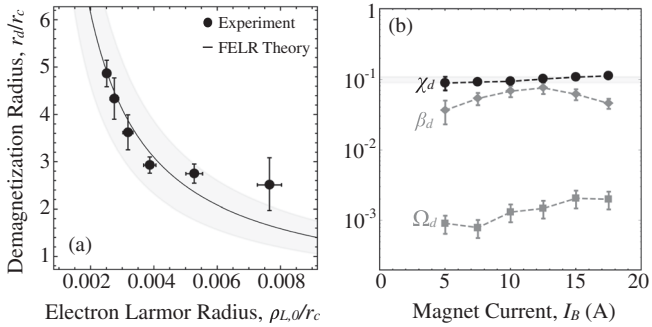

FIG. 5. (a) Demagnetization radius, r_d, versus characteristic electron Larmor radius, $\rho_{L,0}$. Solid line represents the predicted scaling of FELR demagnetization [Eq. (2)] with $\epsilon_\psi^* = 0.04$. (b) Calculated detachment parameters for FELR effects (χ_d), induced magnetic fields (β_d), and electron collisional diffusion (Ω_d).

The physical meaning of ϵ_ψ^* can be explained by noting that $\epsilon_\psi \approx \ell_n/r_p$, where r_p is the local plasma radius and ℓ_n is the distance between ψ_p and ψ_e. For $(r_p/r_0)^2 \gg 1$, $\ell_n \approx \rho_{L,e}$, the local electron Larmor radius. Electron detachment via FELR effects can be examined using the ratio $\chi \equiv \rho_{L,e}/\ell_{\nabla B}$ [10]. We show in Fig. 5(b) the value of χ calculated along ψ_p at r_d, $\chi_d \approx \epsilon_\psi^* r_d/\ell_{\nabla B}$. For comparison, we also show dimensionless quantities that describe the significance of induced magnetic fields, $\beta \equiv 2nk_b T_e/(B^2/\mu_0)$, and electron collisional transport, $\Omega \equiv \nu_e/\omega_{c,e}$, with $\omega_{c,e} = eB/m_e$. Because induced fields create nonlocal effects [45,46], we use centerline measurements to calculate the maximum value of β, defined as β_d. The value of Ω at the detachment point, Ω_d, is estimated using the sum of both electron-ion and electron-neutral collision frequencies, $\nu_e = \nu_{ei} + \nu_{en}$. It is clear from Fig. 5(b) that χ_d is both the most significant and most consistent detachment parameter, supporting our hypothesis that the potential wall disappears due to electron demagnetization via FELR effects. Furthermore, our calculations find $\chi_d = 0.10 \pm 0.01$ to mark the transition into the FELR regime.

Our results provide the first experimental evidence of electron demagnetization via FELR effects in an expanding magnetized plasma. Returning to Fig. 2, we see that demagnetization prior to sufficient thermal-to-kinetic energy conversion can produce rapid plume expansion in MN thrusters, degrading trust efficiency and posing a risk to sensitive satellite equipment. Plume divergence decreases with magnetic field strength because the demagnetization point is pushed further downstream. Setting $r_d = r_{\text{tp}}$ yields a value of $B_0^* \approx 230$ G, where r_{tp} is the turning-point radius of ψ_p. Notably, B_0^* coincides with the field strength at which θ_{div} approaches its asymptotic value (Fig. 2), which suggests MNs should be operated above a critical value of B_0 defined by the inequality $r_d > r_{\text{tp}}$. Finally, we emphasize that the results contained here correlate electron demagnetization to the point where

FELR effects become dominant. Further experimental and theoretical investigation is required to better understand electron dynamics beyond the point of demagnetization.

[1] J. D. Scudder and S. Olbert, J. Geophys. Res. **84**, 6603 (1979).
[2] M. Birkinshaw, Astrophys. Space Sci. **242**, 17 (1996).
[3] D. J. Trevor, N. Sadeghi, T. Nakano, J. Derouard, R. A. Gottscho, P. D. Foo, and J. M. Cook, Appl. Phys. Lett. **57**, 1188 (1990).
[4] Y. Arakawa and A. Sasoh, J. Propul. Power **8**, 98 (1992).
[5] T. Vialis, J. Jarrige, A. Aanesland, and D. Packan, J. Propul. Power **34**, 1323 (2018).
[6] K. Takahashi, Rev. Mod. Plasma Phys. **3**, 3 (2019).
[7] G. Manfredi and R. O. Dendy, Phys. Rev. Lett. **76**, 4360 (1996).
[8] V. Lakhin, V. Ilgisonis, A. Smolyakov, E. Sorokina, and N. Marusov, Phys. Plasmas **25**, 012106 (2018).
[9] H. P. Laqua, Plasma Phys. Controlled Fusion **49**, R1 (2007).
[10] E. Ahedo and M. Merino, Phys. Plasmas **18**, 053504 (2011).
[11] R. W. Moses, Jr., R. A. Gerwin, and K. F. Schoenberg, in *AIP Conference Proceedings* (AIP, College Park, 1992), Vol. 246, pp. 1293–1303.
[12] G. I. Dimov and S. Y. Taskaev, in *Proceedings of the 27th EPS Conference on Controlled Fusion and Plasma Physics, Budapest, Hungary* (American Institute of Aeronautics and Astronautics, Washington, D.C., 2000), ECA Vol. 24B, pp. 464–467.
[13] C. S. Olsen, M. G. Ballenger, M. D. Carter, F. R. C. Diaz, M. Giambusso, T. W. Glover, A. V. Ilin, J. P. Squire, B. W. Longmier, E. A. Bering *et al.*, IEEE Trans. Plasma Sci. **43**, 252 (2015).
[14] S. T. Hepner, T. Collard, and B. A. Jorns, in *2018 Joint Propulsion Conference*, AIAA Propulsion and Energy Forum (American nstitute of Aeronautics and Astronautics, Washington, D.C., 2018).
[15] E. Hooper, J. Propul. Power **9**, 757 (1993).
[16] E. Ahedo and M. Merino, Phys. Plasmas **19**, 083501 (2012).
[17] A. V. Arefiev and B. N. Breizman, Phys. Plasmas **12**, 043504 (2005).
[18] R. Winglee, T. Ziemba, L. Giersch, J. Prager, J. Carscadden, and B. Roberson, Phys. Plasmas **14**, 063501 (2007).
[19] C. A. Deline, R. D. Bengtson, B. N. Breizman, M. R. Tushentsov, J. E. Jones, D. G. Chavers, C. C. Dobson, and B. M. Schuettpelz, Phys. Plasmas **16**, 033502 (2009).
[20] K. Terasaka, S. Yoshimura, K. Ogiwara, M. Aramaki, and M. Tanaka, Phys. Plasmas **17**, 072106 (2010).
[21] K. Takahashi, Y. Itoh, and T. Fujiwara, J. Phys. D **44**, 015204 (2011).
[22] E. Ahedo and M. Merino, Phys. Plasmas **17**, 073501 (2010).
[23] J. M. Little and E. Y. Choueiri, IEEE Trans. Plasma Sci. **43**, 277 (2015).
[24] J. M. Little and E. Y. Choueiri, Phys. Rev. Lett. **117**, 225003 (2016).
[25] I. D. Sudit and F. F. Chen, Plasma Sources Sci. Technol. **3**, 162 (1994).
[26] J. P. Sheehan and N. Hershkowitz, Plasma Sources Sci. Technol. **20**, 063001 (2011).
[27] D. L. Brown, M. L. Walker, J. Szabo, W. Huang, and J. E. Foster, J. Propul. Power **33**, 582 (2017).
[28] L. T. Williams and M. L. R. Walker, IEEE Trans. Plasma Sci. **43**, 1694 (2015).
[29] J. M. Little, Performance scaling of magnetic nozzles for electric propulsion, Ph.D. thesis, Princeton University, 2015.
[30] A. Shabshelowitz and A. D. Gallimore, J. Propul. Power **29**, 919 (2013).
[31] See Supplemental Material at http://link.aps.org/supplemental/10.1103/PhysRevLett.123.145001 for figures containing the ion streamtube locations for different magnetic field strengths and maps of the plasma density, n, and electron temperature, T_e.
[32] J. M. Little and E. Y. Choueiri, Phys. Plasmas **20**, 103501 (2013).
[33] M. Merino and E. Ahedo, Plasma Sources Sci. Technol. **23**, 032001 (2014).
[34] B. W. Longmier, E. A. Bering III, M. D. Carter, L. D. Cassady, W. J. Chancery, F. R. C. Díaz, T. W. Glover, N. Hershkowitz, A. V. Ilin, G. E. McCaskill *et al.*, Plasma Sources Sci. Technol. **20**, 015007 (2011).
[35] K. Takahashi, T. Lafleur, C. Charles, P. Alexander, and R. W. Boswell, Phys. Rev. Lett. **107**, 235001 (2011).
[36] C. Charles, Appl. Phys. Lett. **96**, 051502 (2010).
[37] S. Saha, S. Chowdhury, M. Janaki, A. Ghosh, A. Hui, and S. Raychaudhuri, Phys. Plasmas **21**, 043502 (2014).
[38] M. Merino and E. Ahedo, IEEE Trans. Plasma Sci. **43**, 244 (2014).
[39] J. L. Kline, E. E. Scime, R. F. Boivin, A. M. Keesee, X. Sun, and V. S. Mikhailenko, Phys. Rev. Lett. **88**, 195002 (2002).
[40] S. A. Cohen, N. Siefert, S. Stange, R. Boivin, E. Scime, and F. Levinton, Phys. Plasmas **10**, 2593 (2003).
[41] M. Shoucri, H. Gerhauser, and K.-H. Finken, Comput. Phys. Commun. **164**, 138 (2004).
[42] W. Lee and R. White, Phys. Plasmas **24**, 081204 (2017).
[43] See Supplemental Material at http://link.aps.org/supplemental/10.1103/PhysRevLett.123.145001 for plots of the potential wall strength, Φ_w, versus probe location, z_0.
[44] T. A. Collard and B. Jorns, in *2018 Joint Propulsion Conference*, AIAA Propulsion and Energy Forum (American Institute of Aeronautics and Astronautics, Washington, D.C., 2018).
[45] B. R. Roberson, R. Winglee, and J. Prager, Phys. Plasmas **18**, 053505 (2011).
[46] M. Merino and E. Ahedo, Plasma Sources Sci. Technol. **25**, 045012 (2016).